Cellular and Molecular Life Sciences (2025) 82:96
https://doi.org/10.1007/s00018-025-05577-0

ORIGINAL ARTICLE

Glycocalyx hyaluronan removal-induced increasing of cell stiffness delays breast cancer cells progression

Hui Wang[1,2] · Guoliang Zhang[1] · Yiwen Liu[1] · Yiqing He[1] · Qian Guo[1] · Yan Du[1] · Cuixia Yang[1,2] · Feng Gao[1,2]

Received: 5 June 2024 / Revised: 19 December 2024 / Accepted: 3 January 2025

Abstract

Triple-negative breast cancer (TNBC) cells are rich in glycocalyx (GCX) that is closely correlated with the reorganization of cytoskeletal filaments. Most studies have focused on cell membrane glycoproteins in this context, but rarely on the significance of glycosaminoglycans, particularly the hyaluronan (HA)-associated GCX. Here, we reported that removal of GCX HA could significantly increase breast cancer cells (BCCs) stiffness, leading to impaired cell growth and decreased stem-like properties. Furthermore, we found that the delay of TNBC cells progression could be restored after the cells were re-softened. Meanwhile, in vivo studies revealed that hyaluronidase (HAase)-pretreated BCCs displayed reduced tumor growth and migration. Intriguingly, we identified that ZC3H12A, a zinc-finger RNA binding protein encoded gene, was significantly upregulated after the GCX HA impairment. Of note, knockdown of ZC3H12A could soften the HAase-treated TNBC cells, implying a GCX HA-ZC3H12A regulation on cell stiffening. Taken together, our findings suggested that the breakdown of pericellular HA coat could influence TNBC cells mechanical properties which might be helpful to the future breast cancer research.

Keywords Glycocalyx · Hyaluronan · Cell stiffness · Cell progression · ZC3H12A

Introduction

Cell stiffness is one of the mechanical properties of living cells and plays an indispensable role in maintaining cell shape and characterizing various disorders, including cancer progression, tissue injuries, and inflammations [1, 2]. Accumulating studies demonstrated that circulating tumor cells (CTCs) and metastatic cancer cells are softer than their normal counterparts [3–6]. For example, highly invasive breast cancer cells (BCCs) display a lower cell stiffness [7–9]. Moreover, cell stiffness is thought to be a novel marker for cancer stem cells (CSCs) and cell softening could enhance cancer invasion and migration, which suggest a strong link between cell stiffness and cell malignancy [10, 11]. It is acknowledged that cell membrane shape and cytoskeleton architecture are main regulators of cell stiffness [2, 12, 13]. Of note, the membrane glycocalyx (GCX), a polymer meshwork coating the outside of all living cells, is capable of regulating membrane morphology and inducing cytoskeleton rearrangement [14]. Thus, it is reasonable to speculate that the GCX might be involved in the regulation of cell mechanics. It is well known that the GCX is primarily composed of membrane-bound proteoglycans, sialic acid-containing glycoproteins, glycolipids, and glycosaminoglycans (GAGs) [15]. A previous study has confirmed that mucin, the major membrane glycoprotein, can induce membrane instability and cytoskeleton reorganization [14]. However, few investigations have been focused on the contributions of GAGs in this regard.

The GAGs can be classified into four classes: chondroitin sulfate/dermatan sulfate (CS/DS), heparin/heparan sulfate, keratan sulfate, and hyaluronan (HA) [16]. Recently, it has been acknowledged that the GAGs are involved in tumor growth, progression, metastasis, and invasion [16]. For example, elimination of tumor-associated GCX CS

Hui Wang and Guoliang Zhang contributed equally to this work.

✉ Feng Gao
gaofengly@sjtu.edu.cn

[1] Department of Molecular Biology, Shanghai Sixth People's Hospital, Shanghai Jiao Tong University School of Medicine, 600 Yishan Road, Shanghai 200233, China

[2] Department of Clinical Laboratory, Shanghai Sixth People's Hospital, Shanghai Jiao Tong University School of Medicine, 600 Yishan Road, Shanghai 200233, China

Published online: 27 February 2025

could inhibit prostate cancer cell survival and tumor growth [17]. Besides, researches indicated that highly invasive cancer cells and CTCs enriched with HA matrix in bulky GCX are softer and possess enhanced ability of tumorigenesis and metastasis [18, 19]. Moreover, HA on endothelial cells is believed to be prominent in transducing mechanical forces and inducing cytoskeleton redistribution [20]. These findings prompted us to hypothesize that thicker GCX HA could regulate mechanical properties of cancer cells. Here, we aim to investigate the detailed mechanism underlying GCX HA associated cell stiffness in affecting BCCs activity and survival.

Materials and methods

Cell cultures and treatments

The breast cancer cell lines (MCF10A, T-47D, MCF-7, MDA-MB-468, BT-549, MDA-MB-231, Hs578T, SUM159PT) used in this study were purchased from the Cell Bank of the Type Culture Collection of the Chinese Academy of Sciences and have been authenticated through STR profiling within the last 3 years. All media were supplemented with 10% standard fetal bovine serum (FBS), 1% penicillin/streptomycin (pen/strep) unless otherwise stated. Detailed culture conditions of different cell lines were listed in Supplementary Table 1. All cultured cells were maintained at 37°C in humidified air with 5% CO_2. Basal media, FBS, and pen/strep were all obtained from Gibco.

Bovine testes hyaluronidase (H3506, Sigma, USA) was treated at a final concentration of 500 μg/ml for 24 h. Cyto D (HY-N6682, MedChemExpress, USA) was treated at a final concentration of 0.01 μM for 24 h.

HAS2 knockout and overexpression

Knockout of HAS2 in MDA-MB-231 cells was achieved by co-transfection of the HAS2 CRISPR/Cas9 KO Plasmid (sc-401032) and the HAS2 HDR Plasmid (sc-401032-HDR), which were purchased from Santa Cruz Biotechnology (USA). Transfection procedures were performed using UltraCruz Transfection Reagent (sc-395739, Santa Cruz, USA) according to the manufacturer's instructions. Following a period of 48 h, cells were selected in media containing 2 μg/ml puromycin (ant-pr-1, Invivogen, CA) to obtain MDA-MB-231 HAS2-KO cell line. The HAS2-overexpressed MCF-7 (MCF-7 HAS2-OE) cell line was previously established [21]. The efficiency of HAS2 knockout and overexpression was validated by western blot.

Immunofluorescence

Cells were cultured in 96-well plates with glass bottom, fixed with 4% paraformaldehyde, permeabilized in 0.2% Triton X-100 and blocked with 5% BSA. Then, cells were stained with hyaluronic acid binding protein (HABP, 1:50, 385911, sigma, USA) overnight at 4°C followed by an incubation with Alexa Fluor 594 Streptavidin (1:1000, 35107ES60, YEASEN, Shanghai) for 1 h at room temperature. For the detection of F-actin, cells were stained with Phalloidin-iFluor 647 reagent (1:1000, ab176759, Abcam, UK) for 1 h at room temperature. In addition, vinculin (1:400, V9131, Sigma-Aldrich, USA) and p-paxillin (1:500, 69363, CST, USA) staining were used to detect focal adhesion (FA) of cells. FA numbers and areas were analyzed using the Focal Adhesion Analysis Server (http://faas.bme.unc.edu/) [22]. Images were analyzed under a confocal microscope (Nikon A1, Japan). The line scan intensity analysis of F-actin was performed by Image J software.

Patients and specimens

Specimens were obtained from triple-negative breast cancer (TNBC) and luminal breast cancer patients (10 specimens for each group) according to a standard clinical protocol and were stored at -80°C. The informed consents had been signed by all patients in accordance with the Declaration of Helsinki of the World Medical Association. The study was approved by the ethical committee of Shanghai Sixth People's Hospital Affiliated to Shanghai Jiao Tong University School of Medicine.

AFM indentation assay

In the experiments, the contact mode was carried out with a NanoWizard Sense+ (Bruker, Germany) atomic force microscope (AFM) mounted on an inverted microscope (Olympus IX 81, Japan) on a vibration isolation table. In this study, two different probes were used to perform the indentation assay. One is the MLCT-BIO probe (Bruker) with a triangular tip shape, which has a pre-calibrated spring constant of 0.1 N/m. The other one is the MLCT-SPH-10 μm probe with a 10 μm-radius spherical tip, the spring constant of which is pre-calibrated as 0.104 N/m. We first used the MLCT-BIO probe to conduct force mapping in a 4 μm×4 μm area (25×25 force curves) from over 10 cells for each groups. The cells were maintained at 37°C during indentation using the BioCell (Bruker, Germany). Force mapping images of Young's modulus were acquired by fitting to Hertz model with a tip angle of 19 (half-angle to face) and a poisson ratio of 0.50, which were processed by the JPK SPM Data Processing software.

Then, we utilized the MLCT-SPH-10 μm probe to carry out force spectroscopy experiment from 50 cells (10 curves per cell) for each experimental group. During the indentation assay, we ensured that the applied force was sufficient to induce an indentation range of 1.5–2 μm in the Z length to make sure that the cytoplasm can undergo deformation. Indentation of individual cells was conducted under a piezoactuated displacement rate of 2 μm/s until reaching a set point of constant force (3 nN for MDA-MB-231 cells and 1.5 nN for MCF-7 cells). The cells were maintained at 37°C during indentation. The Hertz model was fit to the approach force-indentation curves to calculate the cellular Young's modulus using the JPK SPM Data Processing software. The Poisson's ratio was taken as 0.5 and the force-indentation curves were plotted by Origin Pro (Ozapin Lab, Northampton, USA).

3D-Structural illumination Microscopy (3D-SIM)

The glycocalyx of the indicated cells was stained with HABP (1:50) directly after fixation overnight at 4°C. Then the cells were incubated with Alexa Fluor 594 Streptavidin at room temperature for 1 h. A 3D-SIM Nikon A1 microscope was used to capture the images with a 100 × oil immersion objective. The measurements of GCX HA thickness were conducted on 20 cells (15 points per cell) from each group. As it was difficult to distinguish the glycocalyx-cytosol boundary of the pseudopodia clearly, we then excluded them from the measurements.

Tumor sphere formation

Cells were seeded on ultra-low attachment 6-well plates (3471, Corning, USA) at a density of 5000 cells/well in DMEM/F12 medium supplemented with B27 (1:50, 12587010, Invitrogen, USA), 20 ng/ml epidermal growth factor (Peprotech, Germany) and 20 ng/ml basic fibroblast growth factor (Peprotech, Germany) for 14 days, media were changed every three days. Then, tumor spheres greater than 50 μm were counted and imaged under an inverted microscope (Olympus, Japan).

Paclitaxel (PTX) sensitivity assay

Cells were seeded on 96-well plates at a density of 5000 cells/well for 24 h and were pretreated with or without hyaluronidase (HAase) for an additional 24 h. Then, various concentrations (5 nM, 10 nM, 20 nM, and 30 nM) of paclitaxel (PTX, HY-B0015, MedChemExpress, USA) were added. After 48 h incubation, the CCK8 reagent (CK04, Dojindo, Japan) was added into each well according to the manufacturer's instructions. The plates were then incubated at 37°C for 2 h to measure the cell viability. The absorbance was measured at 450 nm by a microplate absorbance reader (Bio-Rad Laboratories, Inc).

3D cell migration model

The Matrigel (354234, Corning, USA) was used to construct the 3D cell migration model according to the protocol by prior research [23]. A volume of 50 μl Matrigel was added into the 96-well plate and incubated for 1 h at 37°C. Then, a 50 μl mixture of cell suspension-Matrigel (1:1, 5000 cells/well) was added to each well and cultured at 37°C overnight. Subsequently, the culture medium was added to the plate and cultured for over 48 h until observation by a Nikon Eclipse Ni-U upright microscope (Nikon, Japan).

Wound-healing assay

Cells were grown to 100% confluent in 24-well plates with 10% FBS supplement. Then, the confluent cells were wounded with a sterile pipette tip and washed with PBS to remove the mechanically detached cells. Next, the cells were cultured in FBS-free media and were photographed under a microscope at the indicated time points.

Transwell cell migration assay

Cell migration was assessed using Transwell assay with 8.0 μm pore inserts (Corning, USA) in 24-well plates. A suspension of 5×10^4 cells in media with 1% FBS was seeded onto the upper chamber of the inserts and a volume of 600 μl media containing 10% FBS was layered onto the lower chamber to serve as a chemoattractant. After incubation for an indicated period, non-invasive cells were wiped out with cotton swabs on the upper surface of the membrane. Then, the invasive cells adhered to the lower surface were fixed with 4% paraformaldehyde and stained with crystal violet (Sigma Aldrich, USA). The cell migration was photographed under a microscope and quantified by Image J software.

Colony formation assay

Cells were seeded on 6-well plates (Corning, USA) at a density of 500 cells/well and incubated for 14 days. Next, the cells were washed with PBS, fixed with 4% paraformaldehyde, stained with crystal violet (Sigma Aldrich, USA), and rinsed in purified water. Then, the stained colonies were imaged and counted under an inverted microscope (Olympus, Japan).

Western blot

The western blotting assay was conducted according to the previous description [24]. The primary and secondary antibodies used in the experiment were listed in Supplementary Table 2. The bands were captured by Amersham Imager 680 (GE Healthcare, USA) and the intensity was quantified with Image J software. All procedures were performed in triplicates.

Real-time RT PCR

RNA extraction was conducted using the RNAiso Plus reagent (9108, Takara Bio, Shiga, Japan) and quantified. Then, 1 μg purified RNA was reverse-transcribed into cDNA with PrimeScript™ RT Reagent Kit (RR047Q, Takara, Japan). Real-time PCR experiments were performed with SYBR Green mix (RR820A, Takara, Japan) according to the manufacturer's protocol. All values of genes were normalized against that of GAPDH, and the relative expression of genes was calculated by the $2^{-\Delta\Delta Ct}$ method. The primer sequences used in qPCR were listed in supplementary Table 3.

LUC-lentivirus transduction

MDA-MB-231 control and MDA-MB-231 HAS2-KO cells were transduced with HBLV-zsgreen-luc lentivirus purchased from Hanbio Biotechnology Co. The experimental procedures were performed according to the manufacturer's protocols. Later, the transduced cells were subjected to FACS sorting (MoFlo Astrios EQ; Beckman-Coulter, Inc) and used for xenograft inoculation.

Mouse xenografts tumors

All animal experiment protocols were approved by Institutional Animal Care and Use Committee and all procedures were performed in compliance with relevant laws and institutional guidelines. 15 six-week-old female BALB/c nude mice were purchased from Shanghai Slac Laboratory Animal Co. and were randomly divided into 3 groups: control ($n=5$), HAase ($n=5$), and HAS2-KO ($n=5$). Xenografts were generated by injecting 3×10^6 luciferase-labeled untreated, HAase-pretreated, and MDA-MB-231 HAS2-KO cells into the right mammary fat pads of mice. Tumor length (L) and width (W) were measured weekly using calipers. Tumor volume was calculated using the formula $L\times W^2\times0.5$.

Bioluminescence Imaging

Mice were intraperitoneally injected with 150 mg/kg D-Luciferin (GOLD BIO, USA) 10 min before imaging and were then anesthetized with isoflurane. The entire body and major organs were scanned using an in vivo imaging system (IVIS) 200B (PerkinElmer, Waltham, MA). The bioluminescence images were analyzed using Living Image software 4.7.3 (Caliper Life Sciences).

RNA sequencing and data analysis

RNA sequencing of MDA-MB-231 cells with or without HAase treatment was conducted by an Illumina Novaseq 6000 instrument at the OE Biotech Co., Ltd. (Shanghai, China). FPKM (Fragments Per kb Per Million Reads) of each gene was measured by Cufflinks and the read counts were obtained by HTSeq-count. The DESeq (2012) R package was used to perform differential expression analysis. A fold change greater than 1.5 with a p-value less than 0.05 was defined as the threshold for significantly differential expression.

siRNA transfection

The small interference RNA (siRNA) constructs targeting human ZC3H12A, human RHOD, and human ID1 expression were designed and synthesized by the RiboBio company (Guangzhou, China). The transfection procedures were conducted with riboFECTTM reagents (C11062, RiboBio, China) according to the manufacturer's protocols. The siRNA sequences were listed in Supplementary Table 4.

Statistical analysis

Statistical analysis was performed using GraphPad Prism 8.0.1 (GraphPad Software, Inc). Data were presented as the group mean ± standard deviation (SD). Statistical analysis was performed with unpaired Student's t test for two-group comparisons and one-way analysis of variance (ANOVA) for multigroup comparisons. A p-value less than 0.05 was considered to be statistically significant ($^*p<0.05$, $^{**}p<0.01$, $^{***}p<0.001$).

Results

Triple-negative breast cancer (TNBC) cells display denser GCX HA and are softer than luminal-type BCCs

First, we determined the relationship between GCX HA and BCCs malignancy by immunofluorescent staining. Our results showed that aggressive TNBC cells (MDA-MB-231, BT-549, Hs578T, and SUM159PT), except MDA-MB-468, manifested thicker GCX HA than normal breast epithelial (MCF10A) and luminal (MCF-7, T-47D) cells (Fig. 1a). As HA is synthesized mainly by hyaluronan synthase (HAS), we then examined the expressions of HAS1, 2, 3 at mRNA and protein levels. We found that TNBC expressed a higher level of HAS2 than luminal and normal breast epithelial cells (Fig. 1b, c). However, no significant difference in the expression of HAS1 and HAS3 was observed among these BCCs. Consistently, the level of GCX HA on human TNBC tissues is dramatically higher than luminal ones (Fig. 1d). These data suggested that malignant BCCs were rich in pericellular HA matrices. Given that invasive BCCs are

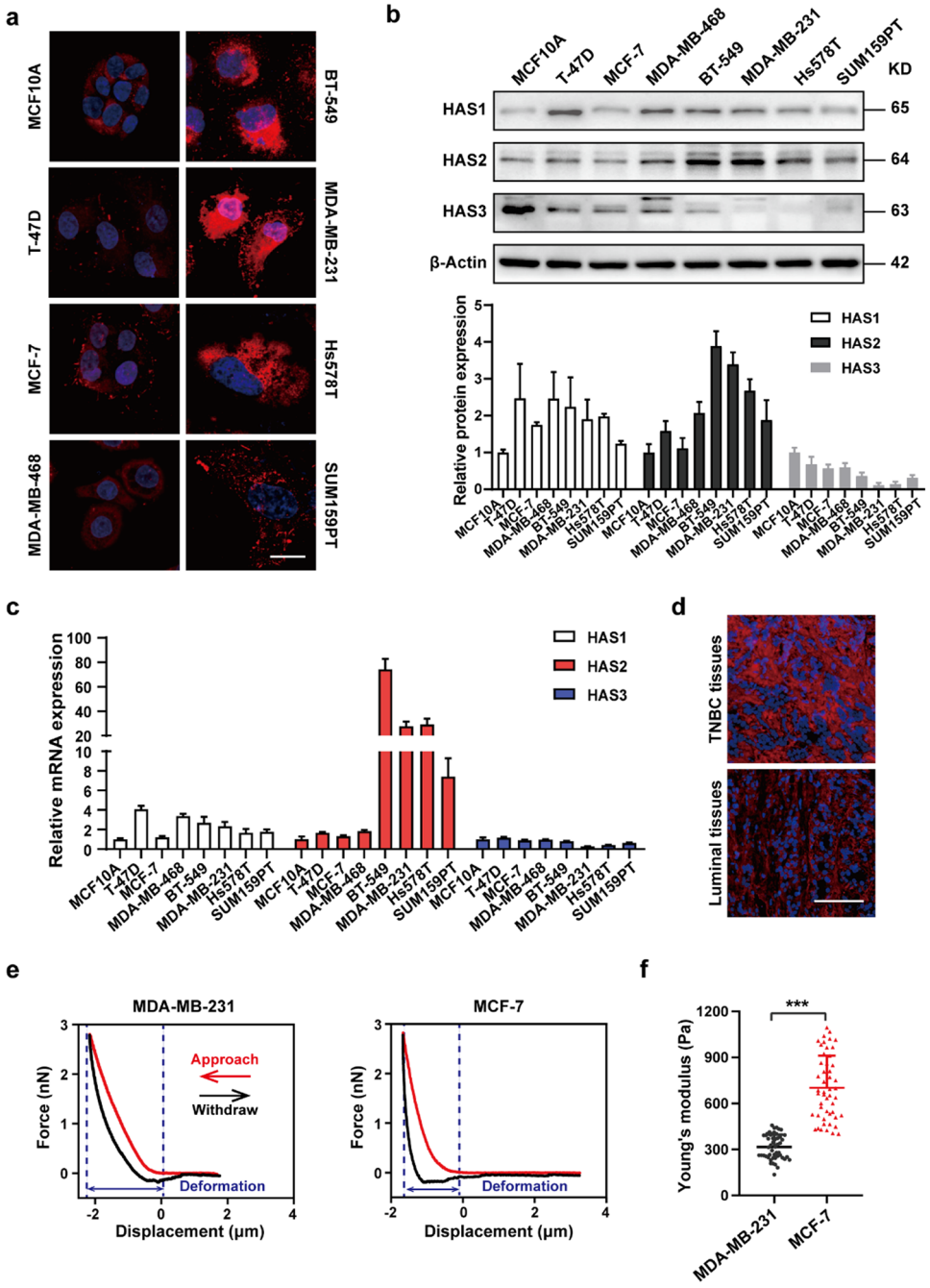

Fig. 1 Triple-negative breast cancer (TNBC) cells display denser GCX HA and are softer than luminal-type BCCs. **a** Immunofluorescent staining with hyaluronic acid binding protein (HABP) (red) in human normal breast epithelial cell (MCF10A), luminal-type BCCs (T-47D and MCF-7), and TNBC cells (MDA-MB-468, MDA-MB-231, BT-549, Hs578T, and SUM159PT). Scale bar, 20 μm. **b-c** Relative protein (b) and mRNA (c) levels of hyaluronan synthase (HAS) 1, HAS2, and HAS3 in the indicated cells. Each bar was presented as the means ± SD of three independent experiments. **d** Representative immunofluorescence staining of HA (red) in human TNBC and luminal-type breast cancer tissues, $n = 10$ independent samples for each group. Scale bar, 100 μm. **e** Representative approach (red) and withdrawal (black) force–indentation curves for MDA-MB-231 and MCF-7 cells measured by atomic force microscope (AFM). Zero indicated the contact point of tip and sample. **f** Young's modulus of indicated cells obtained from fitting the force-indentation curves to Hertz model, $n = 50$ cells for each group, the individual values and means ± SD were plotted, $^{***}p < 0.001$

softer than their benign counterparts and GCX could regulate cytoskeleton reorganization [8, 14], we speculated that GCX HA might be related to cell stiffness. To test this, we next performed AFM nanoindentation experiment to investigate BCCs mechanical properties. By comparing the force-indentation curves of MDA-MB-231 and MCF-7 cells, we found that the slope of the curve in MDA-MB-231 cells was less steep than MCF-7 cells (Fig. 1e, red lines). Moreover, the Young's modulus (calculated by fitting the curves to the Hertz model) of MDA-MB-231 was less than MCF-7 cells (Fig. 1f), implying a decrease in cell rigidity. Collectively, our data suggested that malignant BCCs with denser GCX HA exhibited more softened features.

The breakdown of GCX HA increases cell stiffness

As shown above, HA-rich GCX is negatively related to BCCs stiffness. Given that abundant glycoprotein mucin could induce cytoskeleton rearrangements and plasma membrane instabilities [14], we speculated that a thicker HA coat might influence cell stiffness alteration through eliciting cytoskeleton reassembly underneath the plasma membrane. To explore this, we first investigated the structural configuration of GCX HA on hyaluronidase (HAase)-treated and untreated cells by 3D-SIM and AFM experiments. We found that the thickness of GCX HA was decreased predominantly after HAase treatment under 3D-SIM and IF imaging (Fig. 2a, S1b). In addition, the quantification of the rescaled force curves showed that the long components (L2) of the GCX HA were significantly reduced after HA elimination(978 ± 139 nm for vehicle and 674 ± 51 nm for HAase groups) (Fig. S1c). As HAS2 is recognized as a major contributor in pericellular HA synthesis, we then constructed MDA-MB-231 HAS2-KO, MDA-MB-231 HAS2-overexpression (OE), and MCF-7 HAS2-OE cell lines (Fig. S1a and S4a). Accordingly, the thickness of GCX HA was reduced in MDA-MB-231 HAS2-KO cells (Fig. 2a, S1b, d), whereas opposed results were found in MCF-7 HAS2-OE (Fig. 2a, S1b, e) and MDA-MB-231 HAS2- OE cells (Fig S4b).

To further search for the role of GCX HA remodeling in cell rigidity, we next performed force mapping and spectroscopy experiments for MDA-MB-231 cells with or without GCX HA digestion. We demonstrated that the rupture of the HA coat could significantly increase TNBC cells stiffness (Fig. 2b, e). As expected, similar results were obtained in MDA-MB-231 HAS2-KO cells (Fig. 2c, f), while overproduction of HA in MCF-7 (Fig. 2d, g) and MDA-MB-231 cells (Fig. S4c, d) decreased cell stiffness. As cytoskeleton rearrangement could lead to cell stiffening, we then sought to investigate F-actin distribution after GCX HA reformation. Our results showed that pericellular HA elimination could elicit F-actin bundling underneath the cell membrane (Fig. 2h, i, k). On the contrary, cells with bulkier GCX HA displayed randomly distributed F-actin (Fig. 2j, k, S4e). Taken together, our findings suggested that disruption of GCX HA could increase cell stiffness by inducing cytoskeleton reorganization.

The digestion of GCX HA attenuates TNBC cells stem-like properties

Previous studies demonstrated that tumor cells with lower cell stiffness are highly tumorigenic and metastatic [3, 5, 8]. Our above results indicated that the elimination of GCX HA could increase cell stiffness. These prompted us to investigate whether GCX HA was involved in regulating TNBC cells stem-like properties. First, we performed sphere formation assay and found that the removal of GCX HA remarkably decreased the formation of spheroids compared to the control group in MDA-MB-231 (Fig. 3a, b) and BT-549 (Fig. S3a, b) cells, whereas the overproduction of GCX HA in MCF-7 (Fig. 3c) and MDA-MB-231 (Fig. S4f) cells greatly increased the sphere numbers. In addition, the viability of tumor sphere was assessed by LIVE/DEAD staining dyes. The results showed that over 80% of cells inside a sphere are recognized as live cells (Fig. S2a, b, c). Given that CSC-related genes (Oct4, Sox2, c-Myc, and Nanog) are indicators of stem-like properties, we next explored the expressions of these genes after HA alteration. Our results showed that the expression levels were downregulated upon HA reduction (Fig. 3d, e, S3c), while the overexpressed HA contributed to the opposite results (Fig. 3f, S4g). As tumor resistance towards chemotherapy is one of the stem-like properties, we next conducted paclitaxel (PTX, commonly used for TNBC patients) sensitivity assay to explore whether the GCX HA is correlated with chemosensitivity to PTX. We found that HA depletion enhanced drug susceptibility to PTX (Fig. 3g, h, S3d), while the enrichment of HA showed the reverse results (Fig. 3i, S4h). Collectively, our findings proved that the digestion of GCX HA could attenuate stem-like properties of TNBC cells.

The elimination of GCX HA inhibits cell migration and proliferation in vitro

It is well accepted that enhanced migration and proliferation are features of cancer cell growth and survival. We next tested the contributions of GCX HA to cell progression by 3D culture and transwell migration assays. We found that the elimination of the GCX HA could inhibit cell migration (Fig. 4a, b, d, e, S3f), while the overexpression of HA could promote it (Fig. 4c, f, S4i). Moreover, the results of wound healing assay were in accordance with 3D migration

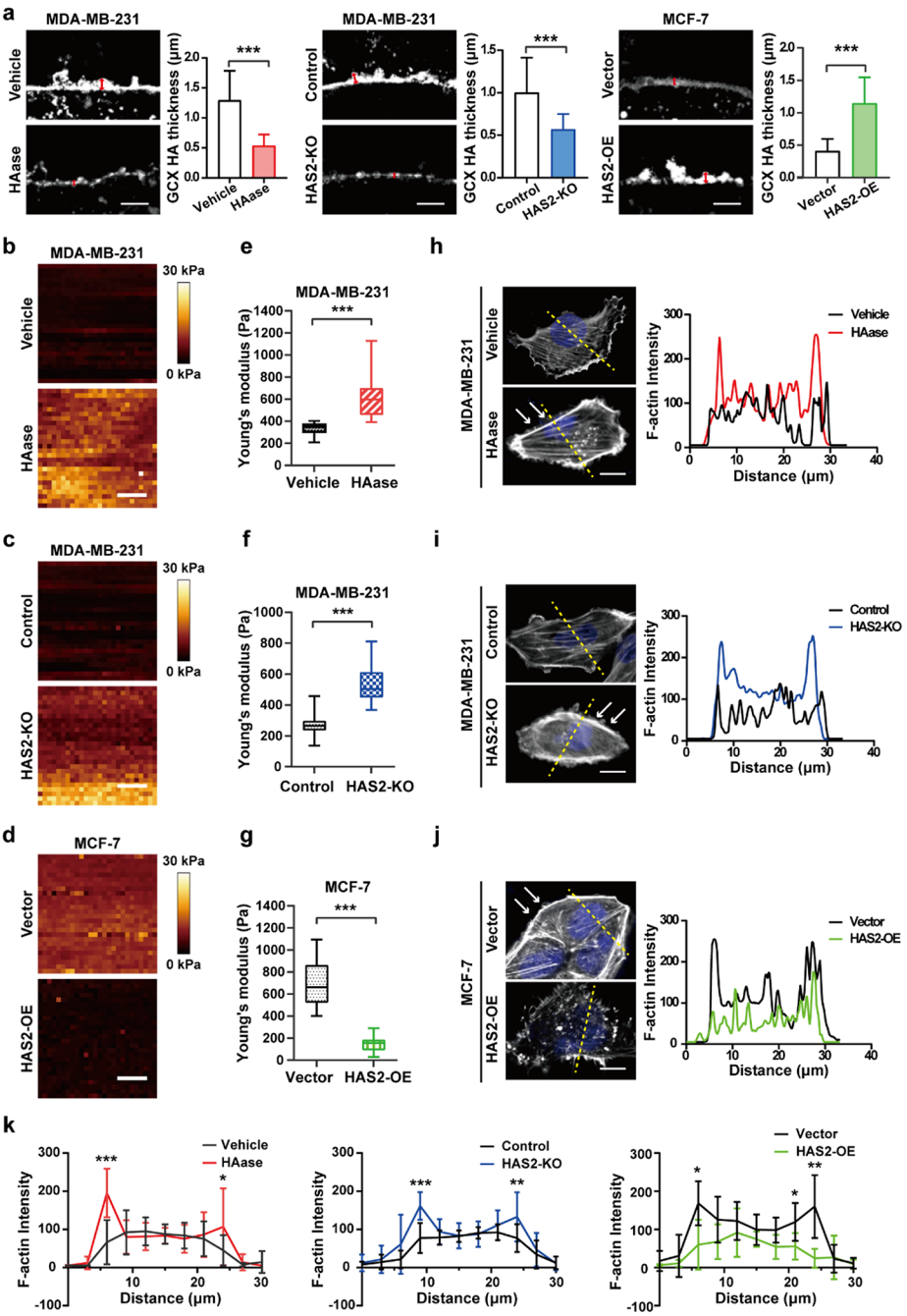

Fig. 2 The breakdown of GCX HA increases cell stiffness. **a** Representative 3D-Structural Illumination Microscopy (3D-SIM) images of indicated cells marked with HABP (white). Scale bar, 2 μm. Quantifications of GCX HA thickness (red arrows) were performed at 20 cells (15 points per cell) for each group. Data were shown as means ± SD, ***$p < 0.001$. **b-d** Representative force-mapping images of Young's modulus. Each image recorded 25 × 25 force-indentation curves within an area of 4 μm × 4 μm on MDA-MB-231 cells with or without HAase treatment (b), MDA-MB-231 HAS2-KO cells (c), and MCF-7 HAS2-OE cells (d), respectively. Scale bar, 1 μm. **e-g** Young's modulus was obtained from fitting the force-indentation curves to Hertz model on MDA-MB-231 cells with or without HAase treatment (e), MDA-MB-231 HAS2-KO cells (f), and MCF-7 HAS2-OE cells (g), respectively. $n = 50$ cells for each group. Data were shown in means ± SD, ***$p < 0.001$. **h-j** Representative immunofluorescent staining of F-actin by phalloidin (white) in the indicated groups with corresponding F-actin line scan (dashed lines in image) intensity analyses. White arrows represented polymerized F-actin underneath plasma membrane. Scale bar, 10 μm. **k** F-actin distribution analysis with line scans (dashed lines) of 10 cells for each group. Each bar was displayed as means ± SD, *$p < 0.05$, **$p < 0.01$, ***$p < 0.001$

(Fig. S2d, e, f, S3e). As focal adhesions (FA) are essential structures that link the intracellular cytoskeleton to the extracellular matrix (ECM), thereby influencing the cancer cells migration [25, 26], we then sought to analyze the roles of GCX HA in affecting FA formation. We found that the removal of GCX HA decreased both FA numbers and areas (Fig. S5a, b, d, e), while the overproduction of GCX HA promoted FA formation (Fig. S5c, f), implying that the GCX HA configuration mediated cell migration is closely related to the FA formation. In addition, the results of the colony formation assay showed that the digestion of pericellular HA could impede cell proliferation (Fig. 4g, h), whereas the enrichment of HA could increase cell survival (Fig. 4i, S3g). Collectively, the impairment of GCX HA could significantly delay TNBC cells growth and migration in vitro.

Re-softening HAase-treated TNBC cells by cytoD promotes cell progression

The above results demonstrated that the elimination of GCX HA could increase cell stiffness and trigger BCCs malignancy reduction as well. In fact, previous studies have

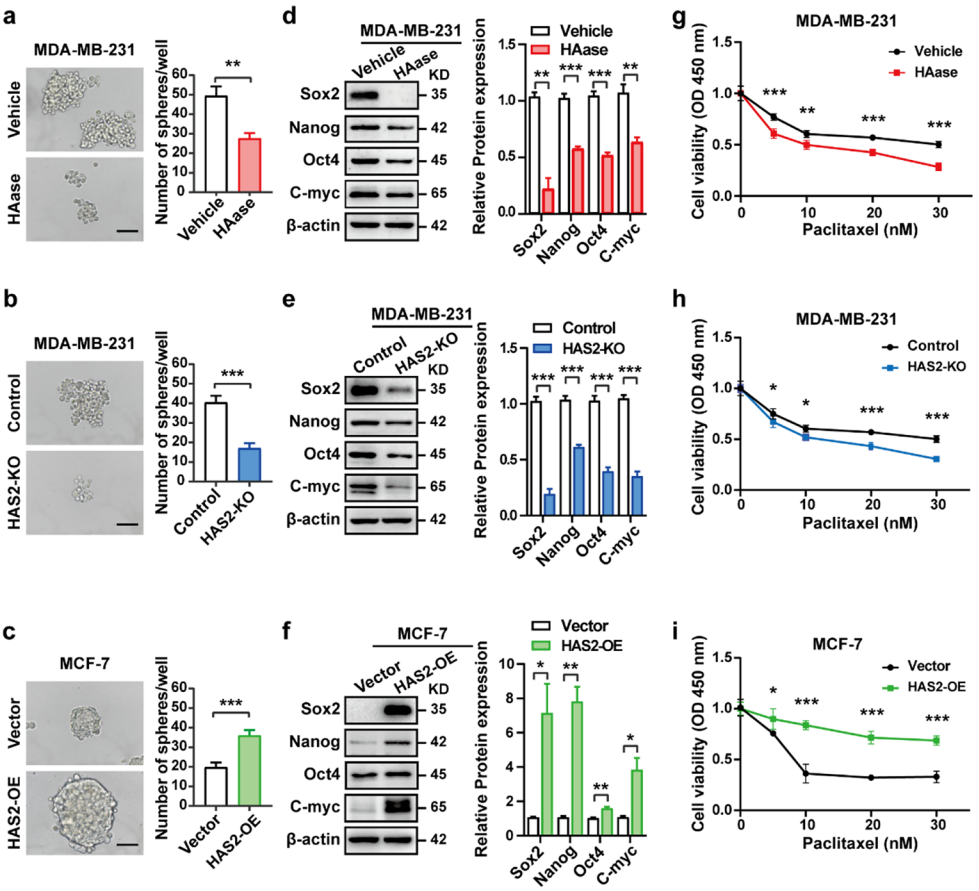

Fig. 3 The digestion of GCX HA attenuates TNBC cells stem-like properties. **a-c** Sphere forming ability of the indicated cells. Scale bar, 100 μm. Numbers of spheres in triplicate experiments were counted and plotted as means ± SD, $^{**}p<0.01$, $^{***}p<0.001$. **d-f** the protein expressions of stemness-related genes (Sox2, Nanog, Oct4, and C-myc) were analyzed in different groups. Each bar was presented as means ± SD of three independent experiments. $^{*}p<0.05$, $^{**}p<0.01$, $^{***}p<0.001$. **g-i** Chemosensitivity to paclitaxel (PTX) of indicated groups at different concentrations. Data were shown as means ± SD with triplicate independent assays, $^{*}p<0.05$, $^{**}p<0.01$, $^{***}p<0.001$

indicated that GCX component mucin could affect F-actin rearrangement, implying a close association between GCX and cell stiffness [10, 11]. We therefore assumed that HA disruption could attenuate TNBC cell progression via inducing cell stiffening. To explore this, we used cytoD, an F-actin polymerization inhibitor, to decrease cell rigidity. We found that cytoD could soften TNBC cells dramatically and impede intracellular F-actin polymerization (Fig. 5a, b, c, d). Importantly, we showed that the Cyto D treatment could effectively increase PTX chemoresistance in HAase-treated MDA-MB-231 cells (Fig. 5e). Consistently, the mammosphere formation (Fig. 5f) and migration (Fig. 5g, h) were recovered after cell re-softening. Taken together, the reduction of GCX HA could increase TNBC cell stiffness, thereby resulting in decreased cell progression.

The depletion of GCX HA inhibits cancer cell growth in vivo

To further validate the function of GCX HA in vivo, we used orthotopic mouse models by implanting untreated, HAase-pretreated, and MDA-MB-231 HAS2-KO cells into the mammary fat pads of BALB/c nude mice. Our results showed that the untreated xenografts grew at a rate evidently faster than the HAase-treated and HAS2-KO ones (Fig. 6a). In addition, weight measurements of tumors at week 7 further verified this difference in tumor growth (Fig. 6b, c). Moreover, micrometastases were observed in the lung and liver tissues of the control group, while no metastatic lesion was observed in the other two HA impairment groups (Fig. 6d, e). Collectively, these results proved that the digestion of GCX HA on the TNBC cells membrane could inhibit tumorigenesis and metastasis in vivo.

The impairment of GCX HA increases cell stiffness via upregulating ZC3H12A expression

Our above data indicated that the remodeling of GCX HA could affect cell progression via altering cell stiffness both in vitro and in vivo. To further unveil the underlying mechanisms, we conducted RNA sequencing assay and highlighted 158 and 176 genes significantly upregulated and downregulated, respectively, in HAase-pretreated MDA-MB-231 cells compared with vehicle ones (Fig. 7a). Among them, ZC3H12A, RHOD and ID1 were demonstrated to be related with cytoskeleton regulation (Fig. 7b). We then investigated the expressions of these three genes in MDA-MB-231 cells, and found that ZC3H12A was upregulated while the other

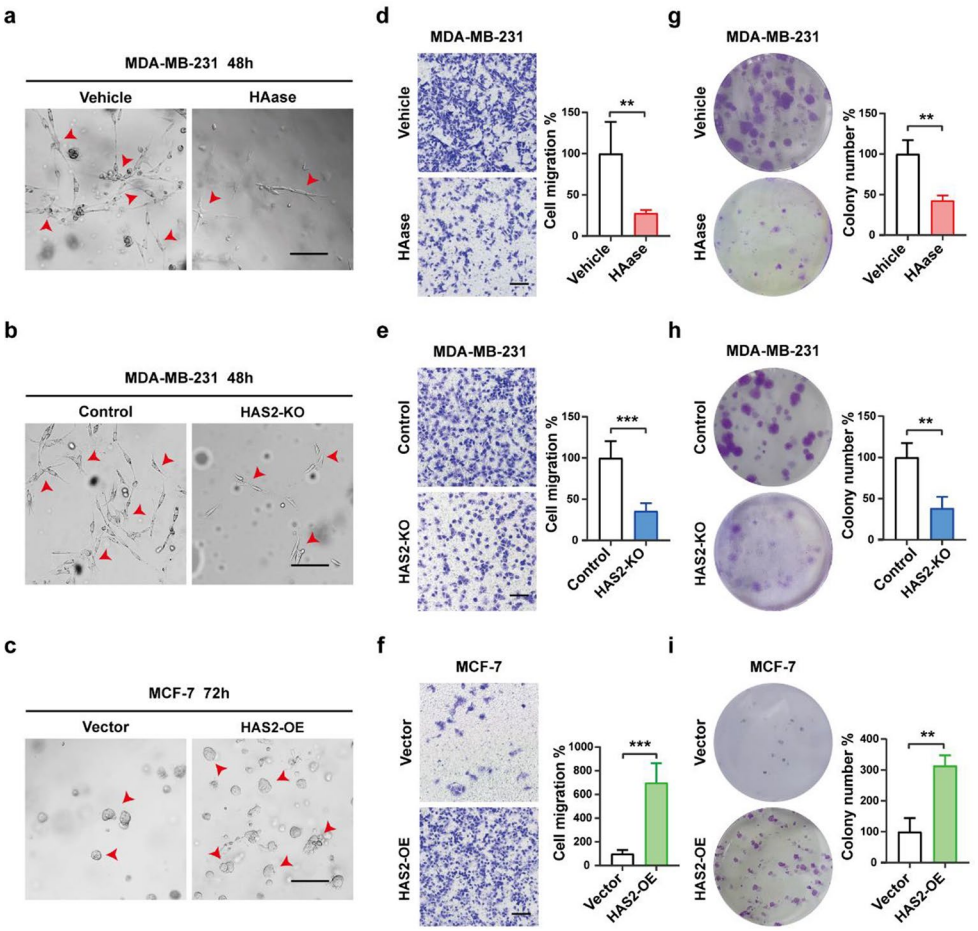

Fig. 4 The elimination of GCX HA inhibits cell migration and proliferation in vitro. **a**-**c** Representative images of 3D cell culture of MDA-MB-231 cells with or without HAase treatment (**a**), MDA-MB-231 HAS2-KO cells (**b**), and MCF-7 HAS2-OE cells (**c**), respectively. Scale bar, 50 μm. **d**-**f** Transwell migration assay for the indicated groups. Scale bar, 100 μm. Each bar represented means ± SD of three independent assays, $^{**}p < 0.01$, $^{***}p < 0.001$. **g**-**i** Colony formation assay for different groups. Data displayed means ± SD of triplicate experiments, $^{**}p < 0.01$

two were downregulated after HAase treatment (Fig. 7c). Furthermore, knocking down ZC3H12A (Fig. S6a) could decrease cell stiffness and abrogate F-actin reorganization induced by HA elimination (Fig. 7d, e, S6b), whereas no difference in this context was found by knocking down RHOD (Fig. 7f, S6c) and ID1 (Fig. 7g, S6d). These results suggested that ZC3H12A might play an indispensable role in mediating HA removal induced cell stiffness augmentation. Collectively, we demonstrated that the digestion of GCX HA on the TNBC cell membrane could upregulate ZC3H12A expression, leading to F-actin bundling and redistribution underneath the plasma membrane.

In conclusion, glycocalyx hyaluronan digestion induced cytoskeleton remodeling may contribute to the increased cell stiffness, resulting in the inhibition of BCCs progression (Fig. 8).

Discussion

While solid tumors like breast cancers are often featured with rigid tissues on palpation, malignant tumor cells are actually softer than their benign counterparts under atomic force microscope (AFM) [5, 27–29]. Moreover, studies reported that breast cancer cells (BCCs) with lower stiffness display enhanced metastasis and stem-like properties [6, 8]. These findings shed light on the significance of mechanical properties of BCCs in cell activities and functions, as well as cancer development. Therefore, unveiling the mechanisms of BCCs behaviors during tumor progression from the perspective of cell mechanics is crucial to the diagnosis and treatment of breast cancers.

The findings of the study

It is demonstrated that dynamic remodeling and rearrangement of cellular cytoskeleton play a pivotal role in modulating cellular stiffness [2, 30]. Moreover, a previous study indicated that mucin, a membrane glycoprotein, could trigger cytoskeleton reorganization and membrane protrusion formation [14]. These findings prompted us to hypothesize that glycocalyx (GCX) on the cell membrane might be involved in modulating cell stiffness via changing the cytoskeletal network. In accordance with our speculation, a recent report demonstrated that hyaluronan (HA), a major component of GCX, could induce endothelial cells cytoskeleton

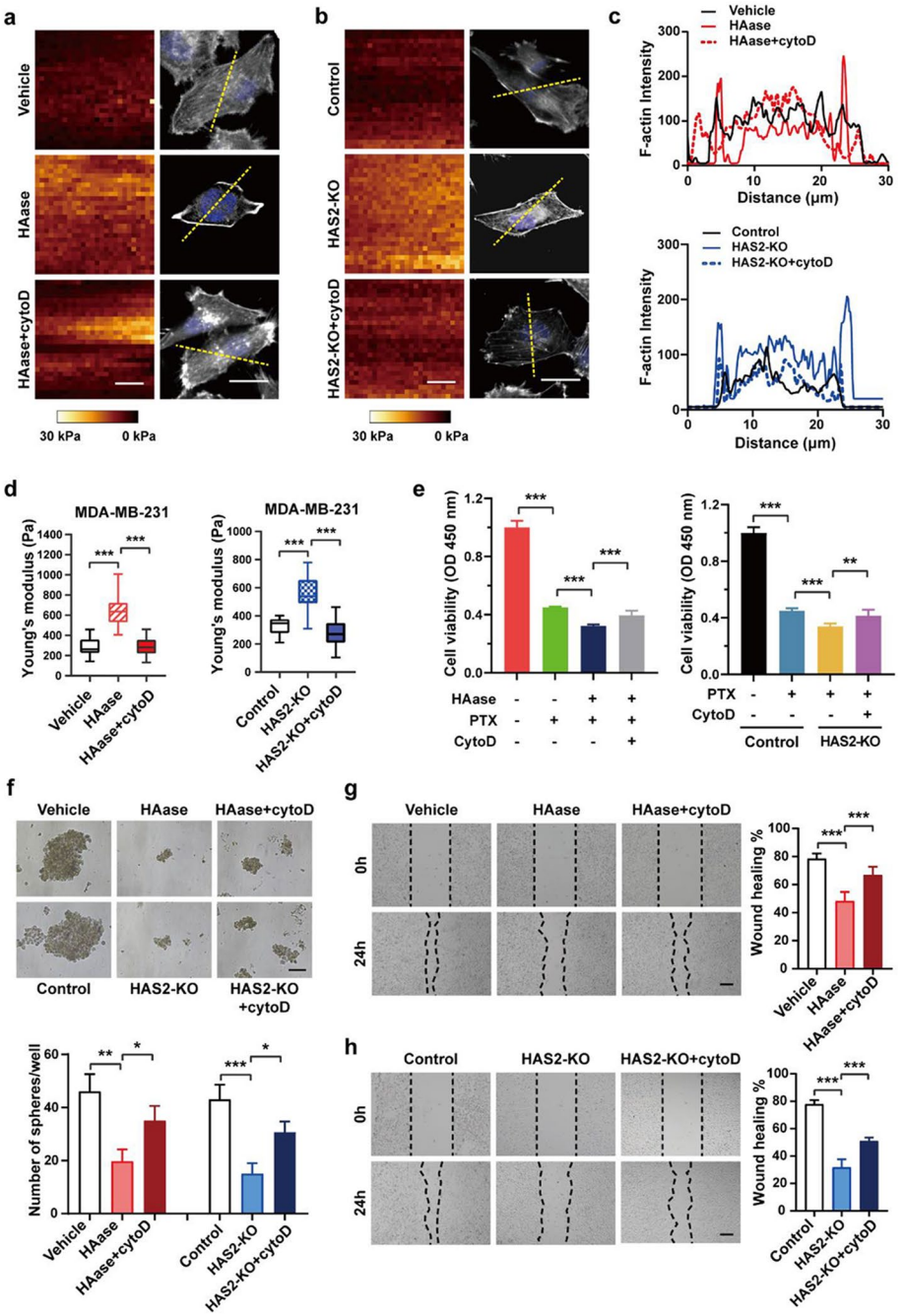

Fig. 5 Re-softening HAase-treated TNBC cells by cytoD promotes cell progression. **a**-**b** Representative force-mapping images of Young's modulus (left panel) and immunofluorescent images of F-actin (right panel) to evaluate the effect of cytoD treatment on HAase-treated MDA-MB-231 cells (**a**) and MDA-MB-231 HAS2-KO cells (**b**). Scale bar, 1 μm for force-mapping images, and 10 μm for immunofluorescent images. **c** Line scan (dashed lines in images) intensity analysis of F-actin. **d** The effect of cytoD treatment on cell stiffness (Young's modulus) of HAase-treated MDA-MB-231 cells (left panel) and MDA-MB-231 HAS2-KO cells (right panel). Young's modulus was calculated from force-displacement curves, $n = 50$ cells for each group. Each bar represented means ± SD, ***$p < 0.001$.**e** The contribution of cytoD treatment to PTX sensitivity in HAase-treated MDA-MB-231 cells (left panel) and MDA-MB-231 HAS2-KO cells (right panel). Data showed means ± SD of triplicate experiments, **$p < 0.01$, ***$p < 0.001$. **f** The effect of cytoD treatment on sphere formation ability in HAase-treated MDA-MB-231 cells (upper panel) and MDA-MB-231 HAS2-KO cells (lower panel). Numbers of spheres in triplicate experiments were counted and plotted as means ± SD, *$p < 0.05$, **$p < 0.01$, ***$p < 0.001$. **g**-**h** the wound closure rate of cytoD treatment in HAase-treated MDA-MB-231 cells (**g**) and MDA-MB-231 HAS2-KO cells (**h**). Data were shown as means ± SD of triplicate experiments, ***$p < 0.001$

alignment in shear-sensing and mechano-transduction in response to shear stress [20]. In addition, another study has reported that thicker GCX HA on highly metastatic cancer cells could contribute to cell survival, anoikis evasion, and chemotherapeutics resistance [31]. However, the exact role of GCX HA in cancer cell mechanics responding to tumor microenvironment remains largely unknown. In this paper, we demonstrated that the elimination of thicker GCX HA on the membrane of TNBC cells could increase cell stiffness via eliciting intracellular F-actin rearrangement. Intriguingly, RNA sequencing analysis showed that ZC3H12A was upregulated upon HA depletion which may be an essential regulator in GCX HA-mediated cell stiffness. Most importantly, this mechanical response by the disruption of GCX HA could attenuate BCCs progression.

The elimination of GCX HA enhances TNBC cells stiffness

In this study, we first determined that malignant TNBC MDA-MB-231 cells are softer than luminal MCF-7 cells, which is consistent with previous findings that highly

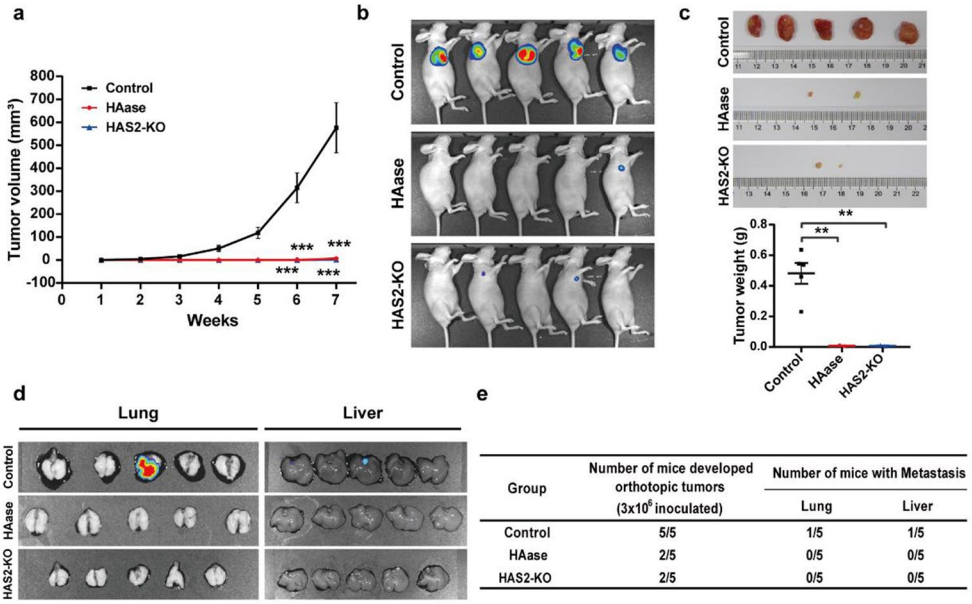

Group	Number of mice developed orthotopic tumors ($3x10^6$ inoculated)	Number of mice with Metastasis	
		Lung	Liver
Control	5/5	1/5	1/5
HAase	2/5	0/5	0/5
HAS2-KO	2/5	0/5	0/5

Fig. 6 The depletion of GCX HA inhibits cancer cell growth in vivo. **a** Tumor formation rate of untreated, HAase-pretreated, and HAS2-KO MDA-MB-231 cells in the orthotopic mammary fat pads of nude mice. The tumor volume was measured as: (Length × Width^2 × 0.5) mm^3 (n = 5/group). Data were shown as means ± SD, ***p < 0.001. **b** Bioluminescence images of xenograft tumors by IVIS imaging system. **c** Images of excised xenograft tumors from mice and the tumor weight was plotted in means ± SD, **p < 0.01. **d** Representative images of lung and liver imaged by IVIS bioluminescence imaging system. **e** The number of mice developed xenograft tumors and metastatic lesions were summarized

aggressive tumor cells are less stiff than their counterparts [5, 8]. As MDA-MB-231 displayed a thicker GCX HA than MCF-7 cells, we further wondered whether there is a correlation between thicker GCX HA and the cell stiffness of BCCs. To address this, we next removed GCX HA by HAase treatment and hyaluronan synthase 2 (HAS2) gene knockout in TNBC cells, and then recovered GCX HA by HAS2 overexpression in luminal MCF-7 cells to investigate the contribution of the GCX HA to cell rigidity. As a result, we found that reduction of GCX HA on TNBC cells could increase Young's modulus under AFM measurement, while the restoration of GCX HA on luminal cells could lead to cell softness, which suggested that the GCX HA remodeling could affect BCCs stiffness.

The decreased cell stiffness is related to BCCs progression

It is reported that a strong reduction of the GCX could influence the membrane bending and change the accessible surface area with substrate nanotopography, which leads to alterations of the actin retrograde flow speed [32]. As cell mechanics are mainly regulated by intracellular cytoskeleton such as F-actin [2], we also found that F-actin was bundled and redistributed underneath the plasma membrane after HA removal during the experiments. Our results are in line with a previous study which demonstrated that actin bundling could mediate cell stiffening in pre-invasive BCCs [12]. Because the cell rigidity is closely related to cancer cell malignancy [15, 18], our findings that GCX HA might influence BCCs stiffness further suggested that GCX HA-dependent BCCs stiffness could regulate cancer cell development.

To confirm our suggestion, we performed series experiments described above, and proved that the HA disruption could decrease TNBC cells proliferation, migration, and stem-like properties, while the GCX HA thickening displayed opposite results. These findings highlighted the significance of GCX HA turnover in regulating cell behaviors, which is supported by a previous report showing that reformation of GCX can impair prostate cancer cells growth and motility [17]. However, the detailed mechanisms of F-actin bundling and redistribution needs in-depth research. For example, a recent study showed that drug-resistant melanoma cells underwent cytoskeletal remodeling via activating ROCK-myosin II pathway to increase cell survival [33]. Because the ROCK-myosin II activity played crucial role in actin dynamics, whether this signaling is involved in GCX HA dependent F-actin remodeling needs our further investigation. Moreover, we also confirmed that the TNBC cells stem-like features could be restored after cell re-softening by using an F-actin polymerization inhibitor. In light of our findings, we concluded that the eliminating of GCX HA could decrease TNBC cells malignancy by increasing cell stiffness.

The in vivo experiment

Encouraged by our in vitro results, we next performed in vivo experiments to evaluate the GCX HA rupture on TNBC cells tumorigenesis. Our results demonstrated that the digestion of GCX HA on MDA-MB-231 cells could dramatically delay tumor xenograft growth in immunodeficient mice, which further provided a support to our in vitro findings. In accordance with our findings, another report has illustrated that intravenous administration of HAase could decrease the

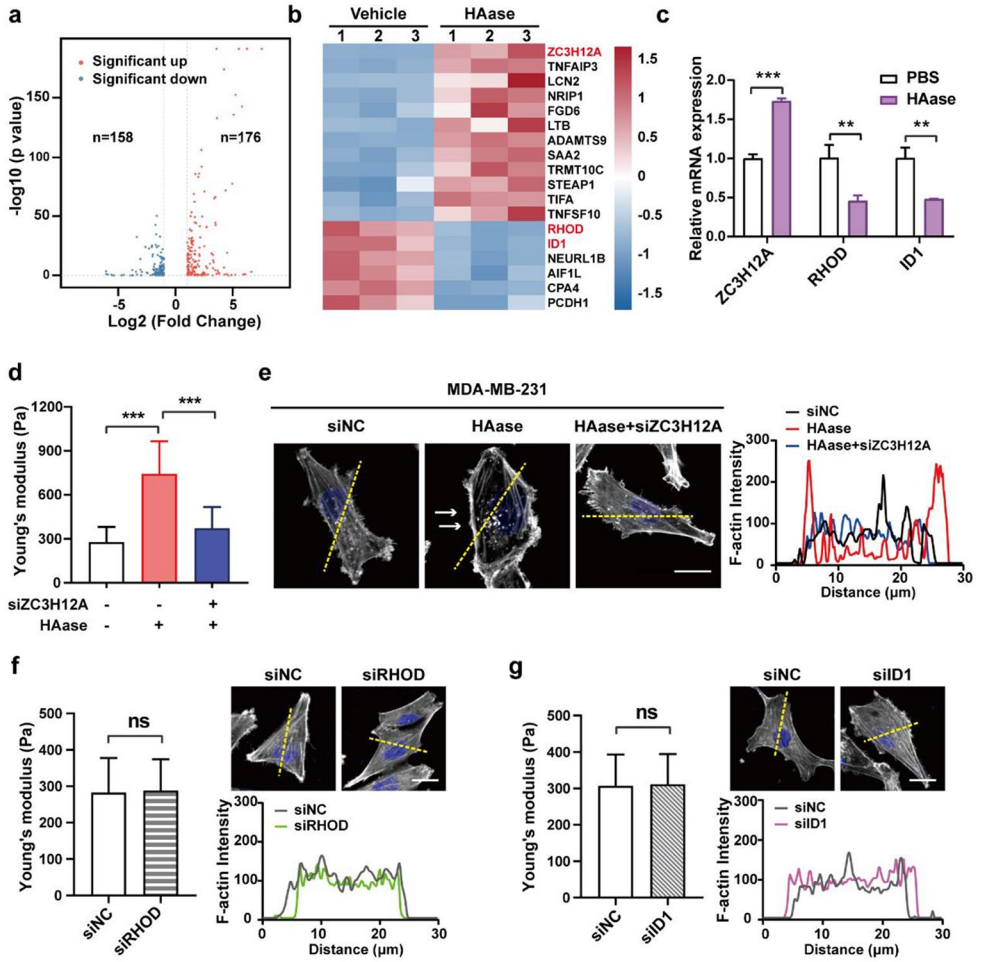

Fig. 7 The impairment of GCX HA increases cell stiffness via upregulating ZC3H12A expression. **a** Volcano plot of log2 fold changes vs. -log10 p-value showed transcriptional differences between HAase-treated and untreated MDA-MB-231 cells. Vertical lines represent the 1.5-fold change cut-off and the horizontal lines indicate the 0.05 *p*-value cut-off. Up- and downregulated genes are highlighted in red and blue, respectively. **b** Heatmap shows expression profiles of the cytoskeleton related genes in HAase-treated and untreated MDA-MB-231 cells. Red colors indicated upregulation, while blue colors represented downregulation. **c** mRNA levels of ZC3H12A, RHOD, and ID1 were tested by qPCR. Data displayed as means ± SD of triplicate experiments, $^{**}p<0.01$, $^{***}p<0.001$. **d** The effects of siZC3H12A on cell stiffness between HAase-treated and untreated MDA-MB-231cells. $n=50$ cells for each group. Data were shown as means ± SD for three independent experiments, $^{***}p<0.001$. **e** Relative F-actin distribution due to ZC3H12A silencing in HAase-treated and untreated MDA-MB-231cells, and F-actin line scan (dashed lines in images) intensity analysis. Scale bar, 10 μm. **f-g** No significant differences were found on cell stiffness and F-actin distribution (dashed lines in images) after siRHOD (**f**) and siID1(**g**) treatment. Each bar presented means ± SD, ns stands for no significance

volume of human breast cancer xenografts in SCID mice by changing the CD44 variant expression [34]. These findings may highlight the significance of in vivo administration of HAase treatment in cancer adjuvant therapeutics. However, there are limitations in our results such as cellular stiffness in vivo has not been measured and the thickness of GCX HA on BCCs was undetected in the process of tumor progression, which need our further research.

The digestion of GCX HA increases cell rigidity via ZC3H12A

To search for the mechanisms underlying HA depletion enhanced cell stiffness, we further performed transcriptional sequencing analysis. We showed that ZC3H12A, a zinc finger RNA binding protein encoded gene, was identified to be robustly upregulated after HAase treatment. As GCX HA removal could attenuate stiffness associated BCCs malignancy, whether the upregulated ZC3H12A was involved in the mechanism of cell stiffness was tested in a knocking down experiment. Our data showed that ZC3H12A

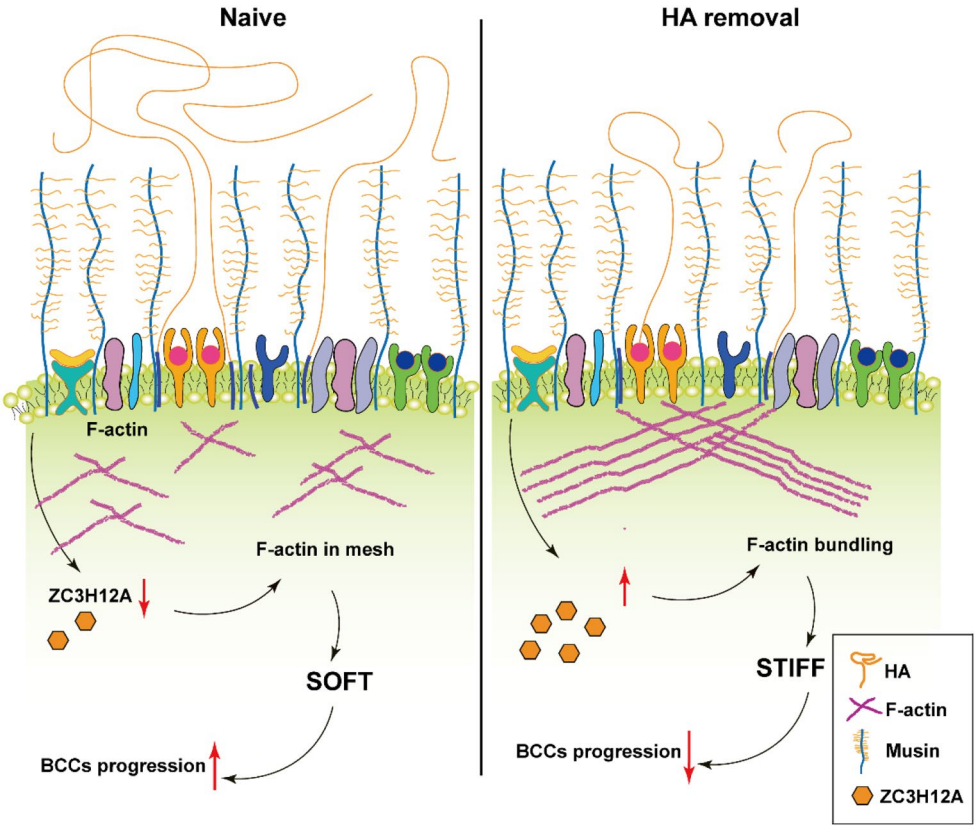

Fig. 8 A schematical model showing the mechanism of GCX HA removal in regulating BCCs stiffness and progression

silencing could significantly soften HAase-treated TNBC cells, implying its role in regulating GCX HA elimination associated cell stiffening. In some related studies, researchers have demonstrated that high ZC3H12A expression was closely associated with longer survival in breast cancer patients [35–37]. Furthermore, as a zinc finger RNA binding protein encoded gene, ZC3H12A is thought to be a fundamental regulator in multiple cellular metabolic processes. For instance, a recent study reported that ZC3H12A could regulate Rho GTPase activity, resulting in actin remodeling [38]. However, the detailed mechanisms how ZC3H12A regulates F-actin rearrangement in our study has not been explored, further research is warranted.

In summary, our work highlights the biological significance of GCX HA in TNBC cells mechanics. Of note, the elimination of GCX HA could increase cell stiffness via ZC3H12A-mediated F-actin rearrangement, resulting in decreased BCCs progression. This study might be valuable to therapeutic interventions aimed at normalizing mechanotransduction in breast cancer treatment.

Supplementary Information The online version contains supplementary material available at https://doi.org/10.1007/s00018-025-05577-0.

Acknowledgements Not applicable.

Author contributions All authors contributed to the conception and design of the studies. HW, GLZ, YWL, YQH, QG, YD, and CXY performed the experiments and analyzed the data. HW, GLZ and FG interpreted the results of the experiments. HW, GLZ prepared figures. HW, GLZ, QG and FG drafted the manuscript. HW, GLZ and FG supervised the study and revised the manuscript. All authors approved the final version of the manuscript.

Funding This work was supported by the National Natural Science Foundation of China (82372710, 82273462, 82073199).

Data availability The data that support the findings of this study are available in the methods and/or supplementary material of this article.

Declarations

Ethical approval All animal experiment protocols were approved by Institutional Animal Care and Use Committee and all procedures were performed in compliance with relevant laws and institutional guidelines.

Competing interests The authors declare no competing financial interests.

References

1. Mierke CT (2022) Viscoelasticity, like forces, plays a role in Mechanotransduction. Front Cell Dev Biology 10. https://doi.org/10.3389/fcell.2022.789841
2. Kwon S, Kim KS (2020) Qualitative analysis of contribution of intracellular skeletal changes to cellular elasticity. Cell Mol Life Sci 77:1345–1355. https://doi.org/10.1007/s00018-019-03328-6
3. Cross SE, Jin Y-S, Rao J et al (2007) Nanomechanical analysis of cells from cancer patients. Nat Nanotechnol 2:780–783. https://doi.org/10.1038/nnano.2007.388
4. Osmulski PA, Cunsolo A, Chen M et al (2021) Contacts with macrophages promote an aggressive Nanomechanical phenotype of circulating Tumor cells in prostate Cancer. Cancer Res 81:4110–4123. https://doi.org/10.1158/0008-5472.CAN-20-3595
5. Gensbittel V, Krater M, Harlepp S et al (2021) Mechanical adaptability of Tumor cells in Metastasis. Dev Cell 56:164–179. https://doi.org/10.1016/j.devcel.2020.10.011
6. Zhang W, Kai K, Choi DS et al (2012) Microfluidics separation reveals the stem-cell-like deformability of tumor-initiating cells. Proc Natl Acad Sci U S A 109:18707–18712. https://doi.org/10.1073/pnas.1209893109
7. Li QS, Lee GYH, Ong CN et al (2008) AFM indentation study of breast cancer cells. Biochem Biophys Res Commun 374:609–613. https://doi.org/10.1016/j.bbrc.2008.07.078
8. Nematbakhsh Y, Pang KT, Lim CT (2017) Correlating the viscoelasticity of breast cancer cells with their malignancy. Convergent Sci Phys Oncol 3. https://doi.org/10.1088/2057-1739/aa7ffb
9. Zbiral B, Weber A, Vivanco MD et al (2023) Characterization of breast Cancer aggressiveness by cell mechanics. Int J Mol Sci 24. https://doi.org/10.3390/ijms241512208
10. Lv J, Liu Y, Cheng F et al (2021) Cell softness regulates tumorigenicity and stemness of cancer cells. EMBO J 40:e106123. https://doi.org/10.15252/embj.2020106123
11. Swaminathan V, Mythreye K, O'brien ET et al (2011) Mechanical stiffness grades metastatic potential in patient tumor cells and in cancer cell lines. Cancer Res 71:5075–5080. https://doi.org/10.1158/0008-5472.CAN-11-0247
12. Tavares S, Vieira AF, Taubenberger AV et al (2017) Actin stress fiber organization promotes cell stiffening and proliferation of pre-invasive breast cancer cells. Nat Commun 8:15237. https://doi.org/10.1038/ncomms15237
13. Tee SY, Fu J, Chen CS et al (2011) Cell shape and substrate rigidity both regulate cell stiffness. Biophys J 100:L25–27. https://doi.org/10.1016/j.bpj.2010.12.3744
14. Shurer CR, Kuo JC-H, Roberts LM et al (2019) Physical principles of membrane shape regulation by the glycocalyx. Cell 177:1757–1770e1721. https://doi.org/10.1016/j.cell.2019.04.017
15. Buffone A, Weaver VM (2020) Don't sugarcoat it: How glycocalyx composition influences cancer progression. J Cell Biol 219. https://doi.org/10.1083/jcb.201910070
16. Morla S (2019) Glycosaminoglycans and Glycosaminoglycan Mimetics in Cancer and inflammation. Int J Mol Sci 20. https://doi.org/10.3390/ijms20081963
17. Al-Nakouzi N, Wang CK, Oo HZ et al (2022) Reformation of the chondroitin sulfate glycocalyx enables progression of AR-independent prostate cancer. Nat Commun 13. https://doi.org/10.1038/s41467-022-32530-7
18. Paszek MJ, Dufort CC, Rossier O et al (2014) The cancer glycocalyx mechanically primes integrin-mediated growth and survival. Nature 511:319–325. https://doi.org/10.1038/nature13535
19. Turley EA, Wood DK, Mccarthy JB (2016) Carcinoma Cell Hyaluronan as a portable Cancerized Prometastatic Microenvironment. Cancer Res 76:2507–2512. https://doi.org/10.1158/0008-5472.Can-15-3114
20. Mylvaganam S, Plumb J, Yusuf B et al (2022) The spectrin cytoskeleton integrates endothelial mechanoresponses. Nat Cell Biol 24:1226–1238. https://doi.org/10.1038/s41556-022-00953-5
21. Zhang G, Guo L, Yang C et al (2016) A novel role of breast cancer-derived hyaluronan on inducement of M2-like tumor-associated macrophages formation. Oncoimmunology 5:e1172154. https://doi.org/10.1080/2162402X.2016.1172154
22. Berginski ME, Gomez SM (2013) The focal adhesion analysis server: a web tool for analyzing focal adhesion dynamics. F1000Res 2:68. https://doi.org/10.12688/f1000research.2-68.v1
23. Li Z, Wang Q, Peng S et al (2020) The metastatic promoter DEPDC1B induces epithelial-mesenchymal transition and promotes prostate cancer cell proliferation via Rac1-PAK1 signaling. Clin Transl Med 10:e191. https://doi.org/10.1002/ctm2.191
24. Qiu Y, Wang H, Guo Q et al (2023) CD44s-activated tPA/LRP1-NFkappaB pathway drives lamellipodia outgrowth in luminal-type breast cancer cells. Front Cell Dev Biol 11:1224827. https://doi.org/10.3389/fcell.2023.1224827
25. Mclean GW, Carragher NO, Avizienyte E et al (2005) The role of focal-adhesion kinase in cancer - a new therapeutic opportunity. Nat Rev Cancer 5:505–515. https://doi.org/10.1038/nrc1647
26. Seetharaman S, Etienne-Manneville S (2020) Cytoskeletal crosstalk in Cell Migration. Trends Cell Biol 30:720–735. https://doi.org/10.1016/j.tcb.2020.06.004
27. Plodinec M, Loparic M, Monnier CA et al (2012) The nanomechanical signature of breast cancer. Nat Nanotechnol 7:757–765. https://doi.org/10.1038/nnano.2012.167
28. Fan L, Strasser-Weippl K, Li JJ et al (2014) Breast cancer in China. Lancet Oncol 15:e279–289. https://doi.org/10.1016/S1470-2045(13)70567-9
29. Alibert C, Goud B, Manneville JB (2017) Are cancer cells really softer than normal cells? Biol Cell 109:167–189. https://doi.org/10.1111/boc.201600078
30. Solon J, Levental I, Sengupta K et al (2007) Fibroblast adaptation and stiffness matching to soft elastic substrates. Biophys J 93:4453–4461. https://doi.org/10.1529/biophysj.106.101386
31. Ahrens TD, Bang-Christensen SR, Jorgensen AM et al (2020) The role of proteoglycans in Cancer Metastasis and circulating Tumor Cell Analysis. Front Cell Dev Biol 8:749. https://doi.org/10.3389/fcell.2020.00749
32. Chighizola M, Dini T, Marcotti S et al (2022) The glycocalyx affects the mechanotransductive perception of the topographical microenvironment. J Nanobiotechnol 20:418. https://doi.org/10.1186/s12951-022-01585-5
33. Orgaz JL, Crosas-Molist E, Sadok A et al (2020) Myosin II reactivation and cytoskeletal remodeling as a Hallmark and a vulnerability in Melanoma Therapy Resistance. Cancer Cell 37:85–103e109. https://doi.org/10.1016/j.ccell.2019.12.003
34. Shuster S, Frost GI, Csoka AB et al (2002) Hyaluronidase reduces human breast cancer xenografts in SCID mice. Int J Cancer 102:192–197. https://doi.org/10.1002/ijc.10668
35. Zhuang J, Wu Y, Chen L et al (2018) Single-cell mobility analysis of metastatic breast Cancer cells. Adv Sci (Weinh) 5:1801158. https://doi.org/10.1002/advs.201801158
36. Lu W, Ning H, Gu L et al (2016) MCPIP1 selectively destabilizes transcripts Associated with an antiapoptotic gene expression program in breast Cancer cells that can elicit complete tumor

regression. Cancer Res 76:1429–1440. https://doi.org/10.1158/0008-5472.CAN-15-1115

37. Chen F, Wang Q, Yu X et al (2021) MCPIP1-mediated NFIC alternative splicing inhibits proliferation of triple-negative breast cancer via cyclin D1-Rb-E2F1 axis. Cell Death Dis 12:370. https://doi.org/10.1038/s41419-021-03661-4
38. Gorka J, Marona P, Kwapisz O et al (2022) MCPIP1 regulates focal adhesion kinase and rho GTPase-dependent migration in clear cell renal cell carcinoma. Eur J Pharmacol 922:174804. https://doi.org/10.1016/j.ejphar.2022.174804